arXiv:1410.6452v1 [cond-mat.supr-con] 23 Oct 2014

On the origin of the electronic anisotropy in iron pnicitde superconductors

W. -L. Zhang,[1,2,*] P. Richard,[2,3] H. Ding,[2,3] Athena S. Sefat,[4]
J. Gillett,[5] Suchitra E. Sebastian,[5] M. Khodas,[6,†] and G. Blumberg[1,7,‡]

[1] *Department of Physics & Astronomy, Rutgers University, Piscataway, New Jersey 08854, USA*
[2] *Beijing National Laboratory for Condensed Matter Physics and Institute of Physics, Chinese Academy of Sciences, Beijing, 100190, China*
[3] *Collaborative Innovation Center of Quantum Matter, Beijing, China*
[4] *Materials Science and Technology Division, Oak Ridge National Laboratory, Oak Ridge, Tennessee 37831-6114, USA*
[5] *Cavendish Laboratory, Cambridge University, JJ Thomson Avenue, Cambridge CB3 OHE, UK*
[6] *Department of Physics and Astronomy, University of Iowa, Iowa City, Iowa 52242, USA*
[7] *National Institute of Chemical Physics and Biophysics, Akadeemia tee 23, 12618 Tallinn, Estonia*

(Dated: October 24, 2014)

We use polarization-resolved Raman spectroscopy to study the anisotropy of the electronic characteristics of the iron-pnictide parent compounds AFe$_2$As$_2$ (A = Eu, Sr) . We demonstrate that above the structural phase transition at T_S the dynamical anisotropic properties of the 122 compounds are governed by the emergence of xy-symmetry critical collective mode foretelling a condensation into a state with spontaneously broken four-fold symmetry at a temperature T^*. However, the mode's critical slowing down is intervened by a structural transition at T_S , about 80 K above T^*, resulting in an anisotropic density wave state.

The properties of solids are defined by the symmetry of the underlying lattice. For the iron pnictide superconductors, the electronic nematicity, a tendency of the electronic ground state to deform spontaneously in proximity to the tetragonal to orthorhombic structural transition, remains the focus of intense research activity [1–3]. In the 122 family of iron pnictides, below the structural transition temperature T_S that breaks the four-fold rotational symmetry, the crystal lattice constants a and b differ by less than one percent while the anisotropy of the electronic characteristics, such as the DC resistivity and the optical conductivity, can be as large as 30 percent [4–6]. More importantly, even above T_S, where the underlying lattice remains tetragonal, large electronic nematic susceptibility has been suggested from resistivity anisotropy measurements in a "zero strain" limit [7] and from the observation of a splitting of the electronic bands derived from degenerate iron orbitals [8, 9]. However, the origin of nematicity remains controversial because of the strong interplay of multiple degrees of freedom.

Theoretical proposals suggest that either the magnetic moments of the iron spins, which order in close proximity to T_S into collinear stripes [3, 10], or the iron d-orbitals, which below T_S no longer have the four-fold symmetry, drive the nematicity [11–13]. Because the tetragonal to orthorhombic transition occurs in close proximity to the magnetic ordering transition (at T_{SDW}) and leads to superconductivity with an unconventional order parameter, in-depth studies of symmetry and critical dynamics of nematic fluctuations are essential to gain an insight into both magnetism and superconductivity in pnictides [3, 14–17].

In this letter we use Raman spectroscopy to study the evolution of electronic anisotropy for representative parent compounds of the iron pnictide superconductors. We demonstrate that critical long temporal collective orbital fluctuations of xy-symmetry develop in a broad range of temperatures, foretelling the new ground state of the same symmetry at temperature T^*. However, condensation into the emergent state is intervened by a first order transition at T_S , about 80 K above T^*, characterized by a broken four-fold symmetry, a doubling of the unit cell, an anisotropic density wave, and a collinear spin stripe order. We propose a microscopic interpretation of the observed anomalous evolution of the Raman susceptibility, elucidate reported anisotropy of electronic characteristics above and below T_S , and explain the implications on superconductivity for doped pnictide materials.

Polarization-resolved inelastic light scattering probes excitations of prescribed symmetries. The temperature evolution of the electronic Raman susceptibility reveals the dynamics of collective excitations and provides an unambiguous identification of their symmetry. Unlike most other symmetry sensitive probes requiring moderate to strong external perturbations, such as magnetic [18] or strain fields [7, 19], the photon field used in Raman scattering is weak. Thus, Raman spectroscopy presents an ideal tool to study the dynamics and symmetry of nematic fluctuations without introducing external symmetry breaking perturbations.

The Raman response function traces electronic density-density correlations driven by the incident and scattered photons of the chosen polarizations ($\boldsymbol{e}^I$ and $\boldsymbol{e}^S$ shown as blue and red arrows in Fig. 1)

$$\chi_{\boldsymbol{e}^I\boldsymbol{e}^S}(\omega) \propto -i\int_0^\infty dt e^{i\omega t}\left\langle[\tilde{\rho}(t),\tilde{\rho}(0)]\right\rangle . \qquad (1)$$

In the effective mass approximation, $\tilde{\rho} = (m/\hbar^2)\sum_{\alpha,\beta} \mathrm{e}^{\mathrm{I}}_\alpha \mathrm{e}^{\mathrm{S}}_\beta \sum_{b,\boldsymbol{k}} \left[\partial^2\epsilon^b_{\boldsymbol{k}}/\partial k_\alpha \partial k_\beta\right] \hat{n}_{b\boldsymbol{k}}$, with m denoting the electron mass and $\hat{n}_{b\boldsymbol{k}}$ the occupation

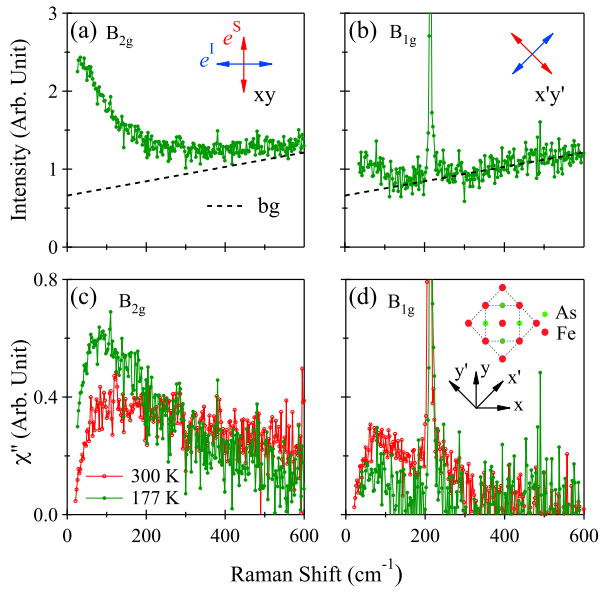

FIG. 1. (color online) Secondary emission (a and b) and Raman response (c and d) for $EuFe_2As_2$ at 177 K (green) and 300 K (red) for xy (a and c) and x′y′ (b and d) polarization geometries corresponding to B_{2g} and B_{1g} responses in the tetragonal phase, recorded with λ_L=476 nm. Schematic diagram of the Fe-As layer is shown in (d), with the tetragonal 2-Fe unit cell in blue and the orthorhombic 4-Fe unit cell in black. The light polarization vectors are denoted with respect to the crystallographic orientations. The luminescence background indicated by black dotted lines in (a) and (b) is determined in Refs. [24, 25].

of the Bloch state at momentum $\boldsymbol{k}$ in the band b with the dispersion $\epsilon^b_{\boldsymbol{k}}$ [20–22]. All components of the symmetrized Raman tensor $\chi_{e^I e^S}$ can be classified by irreducible representations of the crystallographic point group [23]. The two photon fields with cross polarization couple to quadrupole moments, and thus the scattering experiments probe the B_{2g} susceptibility if light polarization is aligned along a and b crystallographic directions, and the B_{1g} susceptibility if rotated by 45°.

For the Fe pnictides, a local charge transfer between degenerate $d_{x'z}$ and $d_{y'z}$ orbitals without a spin flip induces a quadrupole moment of B_{2g} symmetry on an iron site, Fig. 3(b), while no low energy excitation of B_{1g} symmetry is allowed without charge transfer between the irons. Therefore, χ_{xy}, which bears four nodes along the crystallographic directions, delineates such singlet quadrupole excitations [21, 22]. An excitation with a spin flip excites a magnon to which, in the leading order, light cannot couple. In Figs. 3(a-d) we illustrate the relevant quadrupole excitation transition both in k-space and real space.

In Figs. 1(a) and 1(b) we compare the intensity measured in xy and x′y′ geometries [24] from $EuFe_2As_2$ pnictide just above $T_S = 175$ K. The Raman response shown in Figs. 1(c), 1(d) and 2 is derived from the scattering intensity by accounting for the Bose factor [25].

As shown in Fig. 1(d), the electronic response from intraband excitations using the x′y′ polarization is indeed very weak. The broad feature centered at about 75 cm^{-1} is likely due to an interband transitions between the α and β bands, as illustrated in Fig. 3 (a). The sharp mode at 214 cm^{-1} is an iron B_{1g} phonon [26] which only shows weak anomaly upon cooling across T_S [24].

In contrast, the response for the xy polarization is much stronger, the signal extends beyond 1000 cm^{-1}, it strengthens significantly upon cooling and develops a well defined maximum at low energy. In Fig. 2 we show that the temperature evolution of the B_{2g} Raman susceptibility for $EuFe_2As_2$ and $SrFe_2As_2$ is generic for the 122 compounds [27]. Upon cooling toward T_S, the data show gradual enhancement of the low energy response along with linear in temperature softening of the mode maximum frequency from about 160 cm^{-1} at room temperature to 90 cm^{-1} at T_S, denoted $\omega_{max}(T)$ in Figs. 2 (d-e), an energy scale independent on the quasi-particle characteristics. No enhancement with cooling is observed for the susceptibility in any other symmetry channel. Such critical evolution of the anomalous B_{2g} susceptibility due to quadrupole deformation of the electron density at the Fermi surfaces is abruptly intervened at T_S, the entrance into the orthorhombic phase, when a density wave like gap and a coherence peak at about 1070 cm^{-1} develops. The power law in the density wave gap structure suggests that the gap is anisotropic, possibly with a d_{xy} symmetry.

From these data, we calculate and plot in Figs. 2 (d-e) the real part of the static Raman susceptibility using the Kramers-Kronig relations. $\chi'_{xy}(0,T) \propto (T - T^*)^{-1}$ shows a mean-field-like enhancement with temperature T^* about 80 K below T_S. Remarkably, the mode's maximum frequency $\omega_{max}(T)$ scales to the very same $(T-T^*)$ behavior and does not soften near T_S, indicating that the critical slow down is intervened abruptly at T_S.

The B_{2g}-susceptibility data cannot be understood in a picture of non-interacting incoherent quasi-particle excitations because in a paramagnetic phase such excitations can only produce a featureless low frequency response. The spectrum of low-frequency anisotropic plasmas is typically featureless and has a cutoff at $4\pi\hbar v_F/\lambda_L$ due to kinematic constraints of the scattering process, where λ_L is the excitation wavelength and v_F is Fermi velocity in the direction of photon propagation, relatively small for the layered iron pnictides [28, 29]. Hence, the presented $\chi''_{xy}(\omega,T)$ data showing the emergence and softening of an anomalous quasi-elastic response above T_S is a manifestation of electronic correlations.

To describe the observed collective behavior we use an expression for interacting susceptibilities

$$\chi_{xy}(\omega,T) \propto \frac{\chi^{(0)}_{xy}(\omega,T)}{1 - g\chi^{(0)}_{xy}(\omega,T)} \qquad (2)$$

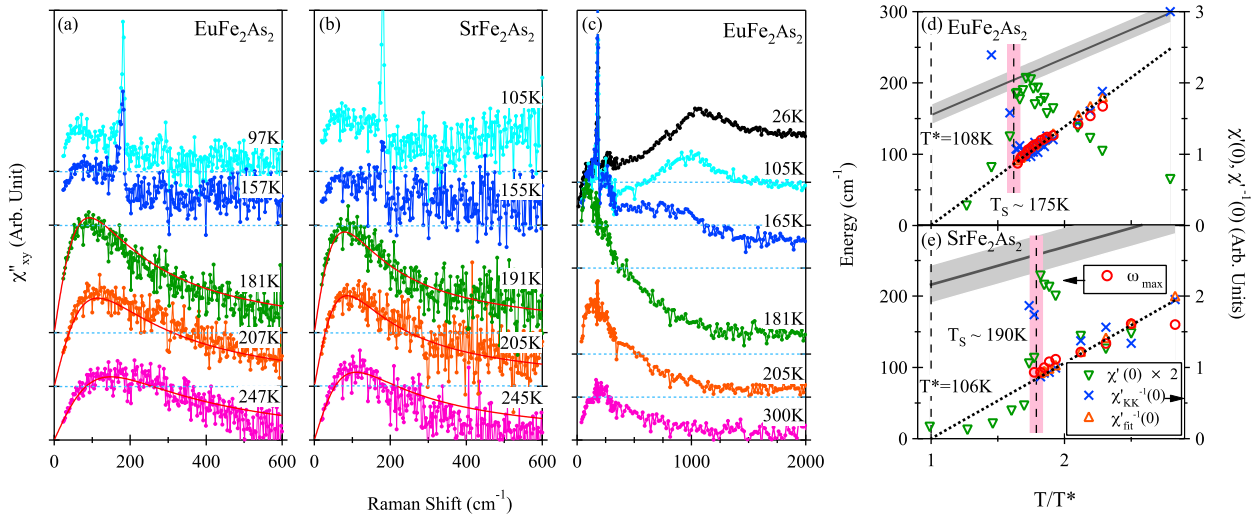

FIG. 2. (color online) Evolution of the Raman response for the xy polarization with cooling from the tetragonal into the orthorhombic phase (a and c) for $EuFe_2As_2$ and (b) for $SrFe_2As_2$. The red curves are the fits to the phenomenological model Eq. (2) [24, 25]. The data show the development of an anomalous quasi-elastic peak above T_S , its abrupt disappearance at T_S , followed by the formation of a density wave gap with a coherence mode at about 1070 cm^{-1} and a new phonon at 183 cm^{-1} . Laser excitations λ_L of 476 nm (a and b) and 647 nm (c) were used. The temperature dependence of the $\chi''_{xy}(\omega,T)$ response maximum $\omega_{max}(T)$ (red circles), of the relaxation rate Γ_T (solid lines, shaded areas indicate the fitting error), the static Raman susceptibility $\chi'_{xy}(0,T)$ (green triangles), $\chi'^{-1}_{KK}(0,T)$ from data (blue crosses), and $\chi'^{-1}_{fit}(0,T)$ from fit (orange triangles) for $EuFe_2As_2$ (d) and $SrFe_2As_2$ (e). The horizontal axis is scaled by T^*. The vertical black dashed lines at $T/T^* = 1.6$ and 1.8 denote T_S , while the red shaded areas indicate an hysteresis.

where $\chi^{(0)}_{xy}$ is the non-interacting susceptibility, and g is the coupling constant. We conjecture

$$\chi^{(0)}_{xy}(\omega,T) = \frac{C}{\pi}\log\frac{(\omega+i\Gamma_T)^2-\Lambda^2}{(\omega+i\Gamma_T)^2}\,, \qquad (3)$$

as this form yields expected featureless bare response $\chi''^{(0)}_{xy}(\omega,T) \propto \arctan(\omega/\Gamma_T)$. Here Γ_T describes a temperature dependent electron-hole relaxation rate $\gtrsim 2k_BT$ and Λ is the ultraviolet cutoff. At $\omega \lesssim \Gamma_T$ Eqs. (3) and (2) yield the relaxational form

$$\chi''_{xy}(\omega,T) \propto \omega\Gamma_T/(\omega_{max}(T)^2+\omega^2)\,, \qquad (4)$$

with $\omega_{max}(T) = \Gamma_T[1/\tilde{g} - \log(\Lambda/\Gamma_T)]$ and $\tilde{g} = Cg$. Because $\chi^{(0)}_{xy}(0,T)$ is logarithmically large, Eq. (2) guarantees the observed critical temperature dependence of the static susceptibility $1/\chi_{xy}(0,T) \propto (1/\chi^{(0)}_{xy}(0,T) - g)$ with T^* defined by the coupling constant g, $\chi^{(0)}_{xy}(0,T^*) = 1/g$.

The expression (2) enables us to fit the entire temperature evolution of the $\chi_{xy}(\omega,T)$ susceptibility between the room temperature and T_S [24]. The data show critical enhancement of the susceptibility and slow down of the characteristic fluctuation frequency $\omega_{max}(T)$, which is abruptly intervened by the structural transition at $T_S \approx 1.6 - 1.8\ T^*$ (See Fig. 2). Above T_S, the observed anomalous temperature dependence of the B_{2g} susceptibility is arising from the critical collective fluctuations indicating the system's approach to a phase transition breaking the four-fold symmetry. The susceptibility reveals how, counteracting the relaxation processes, long temporal correlations characterized by the same symmetry develop, foretelling inception of the new ground state at temperature T^*.

We now turn to the microscopic interpretation of the observed anomalous $\chi_{xy}(\omega,T)$. The body centered unit cell of 122 structure contains two Fe layers with two Fe sites in each one. In the long wavelength limit, B_{2g} and A_{2u} are two possible symmetries of the quadruple excitations, as illustrated in Fig. 3(c-d). The only Raman active quadrupole excitations are singlets of Γ_4^+ (B_{2g}) symmetry. Those quadrupole excitations precipitate the observed anomalous susceptibility. The critical behavior of $\chi_{xy}(\omega,T)$ foretells that the system contemplates a phase transition at temperature T^* which would break the four-fold symmetry without a structural density wave instability and establish the ground state depicted in Fig. 3(c).

For the momentum at the Brillouin zone (BZ) corner, the T_S structural instability vector $X = (\pi/a, \pi/a, 2\pi/c)$, both the singlet quadrupole excitations and the spin triplet excitations obey a degenerate X_5^- symmetry, as illustrated in Figs. 3(e-h). The quadrupole-quadrupole and/or spin-spin interaction between nearest and next-nearest Fe sites favors such collinear stripe order as its ground state [30, 31]. Coupling of quadrupole and spin excitations to the lattice leading to a structural phase transition is naturally expected for non-symmetric fluc-

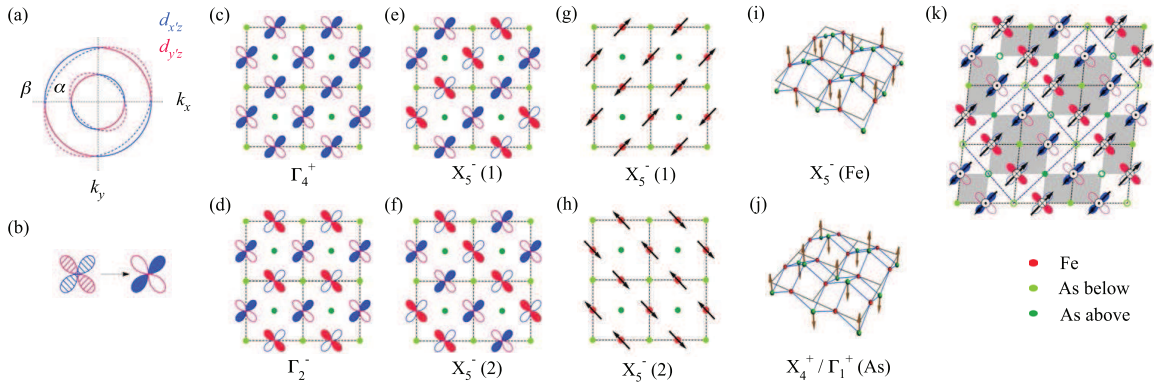

FIG. 3. (color online) (a) Schematic diagram of the α (inner) and β (outer) Fermi surfaces at the BZ center Γ-point. The Fermi surfaces are distorted along the x′ and y′ directions due to the charge transfer fluctuations between the $d_{x'z}$ and $d_{y'z}$ orbitals. (b) A quadruple moment is caused by the charge transfer between the $d_{x'z}$ and $d_{y'z}$ orbitals. (c) and (d) Two possible long wavelength (Γ-point) configurations of quadrupoles with $\Gamma_4^+(B_{2g})$ and $\Gamma_2^-(A_{2u})$ symmetries. In the second Fe layer in the unit cell the $d_{x'z}$ and $d_{y'z}$ orbitals have the same/reversed occupation with the first layer for B_{2g} and A_{2u}, respectively. (e) and (f) The degenerated quadruple excitations that belongs to the X_5^--symmetry at the corner. The second Fe layer has the reversed with the first layer orbital occupation. (g) and (h) The spin triplet excitation that belongs to the X_5^--symmetry at the BZ corner. The second Fe layer has the reversed spin with the first layer. (i) and (j) The atomic displacement of the X_5^- type of Fe and $X_4^+(D_{4h}$ phase)/$\Gamma_1^+(D_{2h}$ phase) type of As shown in one Fe layer. The second Fe layer has the anti-phase/in-phase displacement with the first layer. (k) The possible quadruple, spin and lattice configuration in the orthorhombic ground state below T_S. The Fe X_5^--symmetry displacement. Dots and crosses denote the Fe X_5^--symmetry displacement up and down along the c-direction. The orthorhombic unit cell is shown by the blue dashed line. As ions above and below the Fe layer are distinguished in different colors. The shaded grey rhombuses show a checkerboard charge modulation of approximate xy symmetry.

tuations. If, as it is here, the electronic state is degenerate and can interact with a degenerate lattice displacement, the Jahn-Teller theorem predicts the lifting of the X_5^- quadrupole state degeneracy by interaction with X_5^- phonons [32]. The Fe X_5^- phonon mode, illustrated in Fig. 3(i), buckles the flat Fe layer, modulates the distance between quadrupoles and/or spins and therefore promotes the choice of quadrupole and spin collinear stripe order. The solution of vibronic cooperative $X_5^- \otimes X_5^-$ Jahn-Teller problem results in a new ground state shown in Fig. 3(k). When the lattice symmetry breaks, the quadrupole and spin collinear stripe orders lock-in. Hence, for the parent compounds, the first order structural transition with doubling of the unit cell at T_S, 80 K above T^*, intervenes the formation of the contemplated long-range ordered electronic state. The new order induces long-range charge modulation observed at low temperatures as the d_{xy}-symmetry density wave gap. The distortion of the As layer is induced by coupling to the new electronic ground state of the same symmetry, a quadrupole- and/or magneto-striction, and is revealed by the appearance of the new Raman active As phonon mode below T_S in the spectra of xy polarization, Fig. 2(a-c) and 3(j). As the lattice modulations are buckle-like, the induced anisotropy of the lattice parameters remains weak.

The results obtained here for parent compounds might bear implications on superconductivity in the Fe pnictides. As superconductivity evolves from the tetragonal phase where the B_{2g}-type fluctuations remain dynamic and strong, they may mediate the superconducting pairing of unconventional symmetry, or appear as long-lived in-gap collective modes.

In summary, we use polarization-resolved Raman spectroscopy to study the emergence and the competition of the collective orbital, spin and lattice fluctuations in $EuFe_2As_2$ and $SrFe_2As_2$ parent compounds of the iron pnictide superconductors. In the xy scattering geometry the Raman response exhibits a broad excitation spectrum with a peak at low energy showing critical behavior in a wide temperature range above the structural transition. This spectrum reveals dynamics of the relaxational mode due to orbital fluctuations of B_{2g}-symmetry and demonstrates the general interrelation between anticipated phase transitions breaking the discrete symmetry and critical fluctuations characterized by the same symmetry. For the studded parent compound the condensation of the emergent B_{2g}-mode is intervened by a structural density wave transition characterized by a doubling of the unit cell and a collinear spin stripe order.

We thank Y. Gallais, A. Sacuto, V.-K. Thorsmolle, and Z.P. Yin for fruitful discussions. W.-L.Z. acknowledges ICAM (NSF-IMI grant DMR-0844115) and NSF (DMR-1104884). M.K. acknowledges support

by the University of Iowa. P.R. and H.D. acknowledge MoST (2011CBA001001) and NFSC (11274362) of China. S.E.S. acknowledges ERC (FP/2007-2013)/ERC Grant Agreement no. 337425. A.S.S. and G.B. acknowledge the US DOE, BES and Division of Materials Sciences and Engineering under Awards to ORNL and DE-SC0005463 correspondingly.

* wlzhang@physics.rutgers.edu
† maxim.khodas@gmail.com
‡ girsh@physics.rutgers.edu

[1] E. Fradkin, S. A. Kivelson, M. J. Lawler, J. P. Eisenstein, and A. P. Mackenzie, Annual Review of Condensed Matter Physics **1**, 153 (2010).
[2] J. C. Davis and P. J. Hirschfeld, Nat Phys **10**, 184 (2014).
[3] R. M. Fernandes, A. V. Chubukov, and J. Schmalian, Nature Physics **10**, 97 (2014).
[4] M. Tegel, M. Rotter, V. Wei, F. M. Schappacher, R. Pttgen, and D. Johrendt, Journal of Physics: Condensed Matter **20**, 452201 (2008).
[5] J.-H. Chu, J. G. Analytis, K. De Greve, P. L. McMahon, Z. Islam, Y. Yamamoto, and I. R. Fisher, Science **329**, 824 (2010).
[6] C. Mirri, A. Dusza, S. Bastelberger, J.-H. Chu, H.-H. Kuo, I. R. Fisher, and L. Degiorgi, Phys. Rev. B **89**, 060501(R) (2014).
[7] J.-H. Chu, H.-H. Kuo, J. G. Analytis, and I. R. Fisher, Science **337**, 710 (2012).
[8] M. Yi, D. Lu, J.-H. Chu, J. G. Analytis, A. P. Sorini, A. F. Kemper, B. Moritz, S.-K. Mo, R. G. Moore, M. Hashimoto, W.-S. Lee, Z. Hussain, T. P. Devereaux, I. R. Fisher, and Z.-X. Shen, Proceedings of the National Academy of Sciences **108**, 6878 (2011).
[9] T. Shimojima, T. Sonobe, W. Malaeb, K. Shinada, A. Chainani, S. Shin, T. Yoshida, S. Ideta, A. Fujimori, H. Kumigashira, K. Ono, Y. Nakashima, H. Anzai, M. Arita, A. Ino, H. Namatame, M. Taniguchi, M. Nakajima, S. Uchida, Y. Tomioka, T. Ito, K. Kihou, C. H. Lee, A. Iyo, H. Eisaki, K. Ohgushi, S. Kasahara, T. Terashima, H. Ikeda, T. Shibauchi, Y. Matsuda, and K. Ishizaka, Phys. Rev. B **89**, 045101 (2014).
[10] C. Xu, M. Müller, and S. Sachdev, Phys. Rev. B **78**, 020501(R) (2008).
[11] C.-C. Lee, W.-G. Yin, and W. Ku, Phys. Rev. Lett. **103**, 267001 (2009).
[12] H. Kontani, Y. Inoue, T. Saito, Y. Yamakawa, and S. Onari, Solid State Communications **152**, 718 (2012).
[13] S. Onari and H. Kontani, Phys. Rev. Lett. **109**, 137001 (2012).
[14] C. Fang, H. Yao, W.-F. Tsai, J. Hu, and S. A. Kivelson, Phys. Rev. B **77**, 224509 (2008).
[15] P. J. Hirschfeld, M. M. Korshunov, and I. I. Mazin, Reports on Progress in Physics **74**, 124508 (2011).
[16] R. M. Fernandes, A. E. Böhmer, C. Meingast, and J. Schmalian, Phys. Rev. Lett. **111**, 137001 (2013).
[17] R. M. Fernandes and A. J. Millis, Phys. Rev. Lett. **111**, 127001 (2013).
[18] S. Kasahara, H. Shi, K. Hashimoto, S. Tonegawa, Y. Mizukami, T. Shibauchi, K. Sugimoto, T. Fukuda, T. Terashima, A. H. Nevidomskyy, *et al.*, Nature **486**, 382 (2012).
[19] X. Lu, J. T. Park, R. Zhang, H. Luo, A. H. Nevidomskyy, Q. Si, and P. Dai, Science **345**, 657 (2014).
[20] M. V. Klein, Phys. Rev. B **82**, 014507 (2010).
[21] C. Sauer and G. Blumberg, Phys. Rev. B **82**, 014525 (2010).
[22] I. I. Mazin, T. P. Devereaux, J. G. Analytis, J.-H. Chu, I. R. Fisher, B. Muschler, and R. Hackl, Phys. Rev. B **82**, 180502 (2010).
[23] L. N. Ovander, Optics and Spectroscopy **9**, 302 (1960).
[24] See Supplementary Information.
[25] $I_{\rm xy}(\omega,T)=\chi''_{\rm xy}(\omega,T)(1+n_{\omega,T})+I_{bg}$ is used to describe the Raman response and the background for spectra at all temperatures. $n_{\omega,T}$ is the Bose Einstein distribution temperature factor. The background function $I_{bg}=a+b\omega+cT$ while a, b and c are fitting parameters. For one particular compound all the coefficients namely a, b, c, α and $\Gamma_{\rm res}$ are kept constant for all temperatures in the nematic fluctuating phase.
[26] A. P. Litvinchuk, V. G. Hadjiev, M. N. Iliev, B. Lv, A. M. Guloy, and C. W. Chu, Phys. Rev. B **78**, 060503 (2008).
[27] Y. Gallais, R. M. Fernandes, I. Paul, L. Chauvière, J.-X. Yang, M.-A. Méasson, M. Cazayous, A. Sacuto, D. Colson, and A. Forget, Phys. Rev. Lett. **111**, 267001 (2013).
[28] P. M. Platzman, Phys. Rev. **139**, A379 (1965).
[29] M. V. Klein and S. B. Dierker, Phys. Rev. B **29**, 4976 (1984).
[30] P. Chandra, P. Coleman, and A. I. Larkin, Phys. Rev. Lett. **64**, 88 (1990).
[31] R. M. Fernandes, L. H. VanBebber, S. Bhattacharya, P. Chandra, V. Keppens, D. Mandrus, M. A. McGuire, B. C. Sales, A. S. Sefat, and J. Schmalian, Phys. Rev. Lett. **105**, 157003 (2010).
[32] I. B. Bersuker, Chem. Rev. **101**, 1067 (2001).